Chopper-Stabilized Bidirectional Current Acquisition Circuits for Electrochemical Amperometric Biosensors

Hamed Mazhab Jafari and Roman Genov

Abstract—**Two low-noise bidirectional current acquisition circuits for interfacing with electrochemical amperometric biosensor arrays are presented. The first design is a switched-capacitor transimpedance amplifier (TIA). The second design is a current conveyer (CC) with regulated-cascode current mirrors. Both circuits employ chopper stabilization to reduce flicker noise. The TIA and the CC were prototyped in 0.13 μm CMOS and consume 3 μW and 4 μW from a 1.2 V supply, respectively. The electrical and electrochemical recording properties of both circuits have been characterized. The current conveyer exhibits superior performance in low-concentration electrochemical catalytic reporter sensing, as less switching noise is injected into the biosensor.**

Index Terms—**Bidirectional current, biosensor, current conveyer, cyclic voltammetry, electrochemical sensor, transimpedance amplifier.**
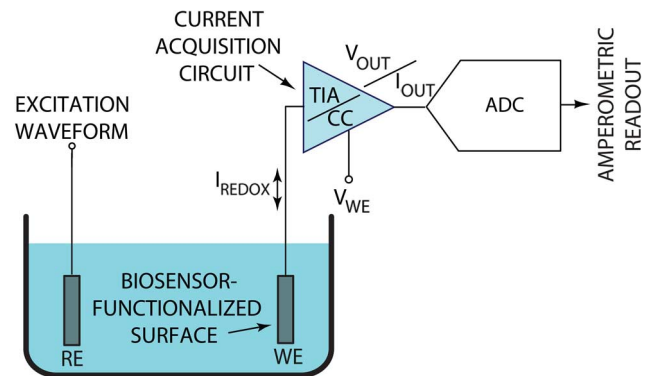
I. INTRODUCTION

S EVERAL promising sensory interfaces for biological and chemical sensing applications have been introduced in recent years, such as sensory systems for monitoring of chemical neural activity of the brain [1], [2] and for DNA detection [3]–[9]. Electrochemical amperometric sensing is gaining popularity in such applications [10], [11].

A block diagram of an electrochemical amperometric sensing system is shown in Fig. 1 [10]. The electrochemical cell consists of a working electrode (WE) and a reference electrode (RE). The current acquisition circuit holds the working electrode at a known potential and records the reduction-oxidization (redox) current generated due to the voltage difference between the working and reference electrodes. Two common types of current acquisition circuits are a transimpedance amplifier (TIA) and a current conveyer (CC) that generate a voltage and a current, respectively, at the output as shown in Fig. 1.

A generic $R - C$ biosensor impedance model is depicted in Fig. 2. In this model R_S represents the electrolyte resistance between the working and reference electrodes, C_{WE} represents the diffusion layer capacitance, C_{DB} models the interfacial double-layer capacitance at the WE-electrolyte interface and

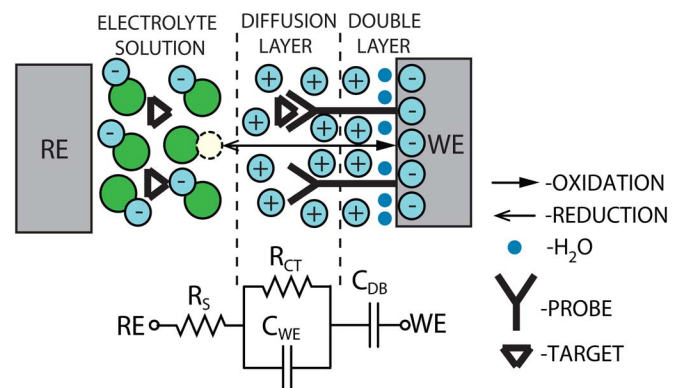Fig. 1. Conceptual view of an electrochemical amperometric sensory system.

Fig. 2. Charge profile of the electrode-electrolyte interface and its equivalent circuit model.

R_{CT} models the charge transfer resistance at the WE-electrolyte interface [11]. The double-layer consists of solvated positive ions physically separated from the working electrode surface by a monolayer of water molecules and ions at the working electrode surface. Biochemical probes, biologically active compounds such as artificial antibodies, enzymes or receptors, are integrated with the working electrode. The diffusion layer is the layer beyond the double layer where the capturing probe molecules are located [12]. The integration process is performed by the immobilization and stabilization of biological sensor molecules on the electrode surface. For example, in DNA sensing applications the surface of the working electrode is functionalized with probe DNA. Binding of the probe DNA with the matching target DNA results in a change of the working electrode surface properties such as impedance and
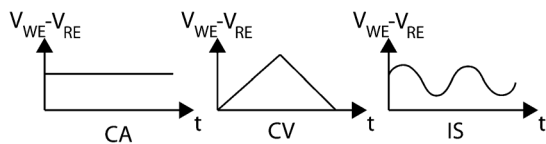
Fig. 3. Electrode voltage waveform for the three electrochemical amperometric sensory methods: constant potential amperometry (CA), cyclic voltammetry (CV) and impedance spectroscopy (IS).

surface charge amount. The variation of the surface properties results in a change in the recorded value and waveform features of the redox current flowing through the working electrode, thus indicating the thermodynamics and kinetics of chemical reactions at the sensory interface indicative of the presence and concentration of the target DNA. In most biochemical sensing applications the recorded redox current is in the range of low pAs to low nAs and the biosensor frequency response covers a range of 1 Hz to 1 kHz [10].

An example of the mechanism of generation of the redox current is also shown in Fig. 2. In the presence of a potential difference between the working electrode and the reference electrode the electroactive chemical species of the electrolyte solution are either reduced (gain an electron) or oxidized (loss an electron). The amount of charge transferred between the electrolyte solution and the working electrode depends on the surface charge. The surface charge in turn depends on the density of the target molecules that have bound to probes. Measuring the current corresponding to the charge transfer yields a measures of the concentration of the target molecules.

The reference electrode is set to a constant voltage for constant-potential amperometry (CA), a bidirectional ramp voltage for cyclic voltammetry (CV), or a small-amplitude sinusoid for impedance spectroscopy (IS) as shown in Fig. 3. The constant-potential amperometry method provides high sensitivity at the cost of limited selectivity. The cyclic voltammetry method provides lower sensitivity compared to the CA method but it is highly selective. A drawback of this method is the creation of a large background current due to the dynamic nature of CV waveforms. The background current can be orders of magnitude larger than the redox current. This places a stringent requirement on the dynamic range of the current acquisition circuit. A drawback of the IS method compared to the CV and CA methods is the long time required for acquiring a biosensor spectrum which can affect the real-time detection capability.

The use of a transimpedance amplifier is the most common approach to redox current acquisition [10]. In this approach the transimpedance amplifier (TIA) sets a virtual potential at the working electrode and at the same time generates an output voltage that is proportional to the redox current. This can be implemented as a resistive feedback configuration [13] or a switched-capacitor circuit [14]. The size of the resistors in the resistive feedback configuration makes it impractical for massively-parallel array sensing implementations. Additionally in a resistive feedback configuration the thermal noise can be injected back into the biosensor. The switched-capacitor TIA configuration is a common choice for arrayed implementations [7].

A current conveyer (CC) is another common compact circuit for measuring the redox current [17]. The WE is held at a virtual potential. Instead of converting the redox current directly to voltage, it is conveyed from WE to a high-impedance output node and can then be converted to a voltage. A number of current conveyer designs for amperometric sensing applications have been reported [16]–[21].

We present a study of the utility of the switched-capacitor TIA and CC circuits in acquisition of bidirectional currents in electrochemical amperometric biosensing applications. Advantages and disadvantages of the TIA and CC circuits in such applications are described and experimentally confirmed. This work builds on the theoretical noise analysis presented in [22], [23]. Specifically, we show that the main drawbacks of the switched-capacitor TIA is the injection of the the switching noise into the sensor working electrode. The switching noise injected into the working electrode alters the charge at the working electrode surface, thus degrading the electrochemical recording results accuracy.

We introduce a solution to this problem, a low-noise bidirectional current conveyer for small currents. The advantage of this method, compared to a transimpedance amplifier, is that the working electrode is isolated from the clocked circuitry (e.g, switches, ADC, comparator) thus reducing the effect of charge injection into the working electrode due to high-frequency switching. Generally current conveyers suffer from the amplifier flicker noise as it is not integrated as in the case of the TIA. Internal OTA chopper stabilization is utilized to reduce the effect of the flicker noise, the dominant noise of the amplifier. The CC achieves a dynamic range of 8.6 pA to 350 nA. Finally, we present a comparative analysis of a bidirectional-input TIA and a bidirectional CC fabricated in 0.13 μM CMOS technology.

This paper extends on an earlier report of the current conveyer design presented in [15], and offers a more detailed analysis of the design and additional electrochemical experimental results characterizing the circuit implementation and comparing the current conveyer implementation to a transimpedance amplifier implementation for electrochemical recording. The rest of the paper is organized as follows. Section II presents the TIA design and implementation and includes experimentally measured results. Section III details the circuit implementation of the CC and also includes experimentally measured results. Section IV presents a comparative analysis of the TIA and CC designs and their utility in electrochemical sensing applications.

II. TRANSIMPEDANCE AMPLIFIER (TIA)

As described in Section I, most electrochemical biosensing applications require sourcing and sinking the redox current. One way to measure a bidirectional redox current is to directly convert it to a voltage. The conversion can be done by a resistive or a capacitive feedback across an OTA, known as a transimpedance amplifier (TIA). To convert a low-level current in the nano-ampere or pico-ampere range, a very large resistor is required. A capacitive feedback allows to keep the area small. In addition, a capacitive TIA has an averaging behavior and acts as a low-pass filter to remove the high-frequency noise [14].
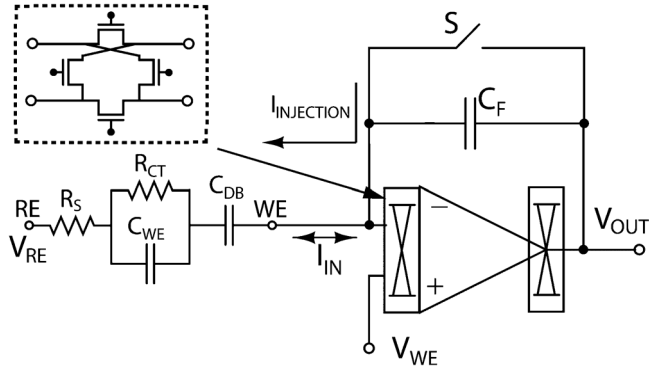
Fig. 4. Chopper-stabilized bidirectional-input transimpedance amplifier (TIA).

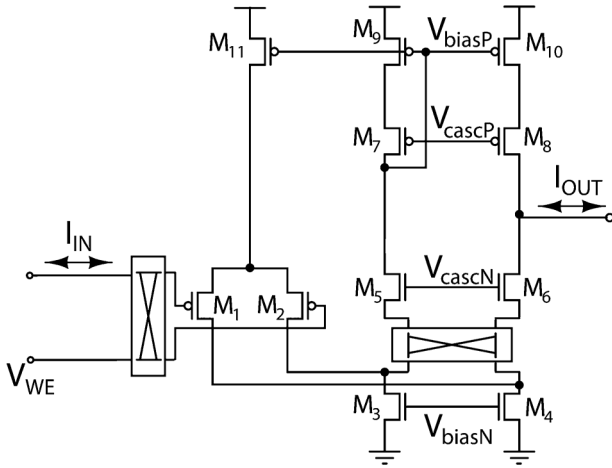
Fig. 5. Circuit schematic diagram of the OTA within the TIA.
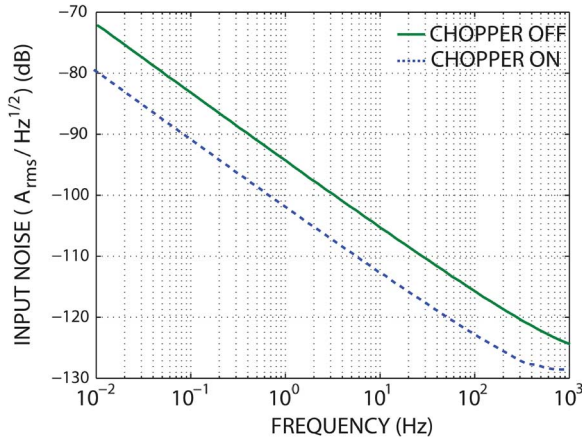
Fig. 6. Simulated input-referred noise spectrum of the TIA from 0.01 Hz to 1 kHz.

TABLE I
TIA OTA TRANSISTORS SIZING

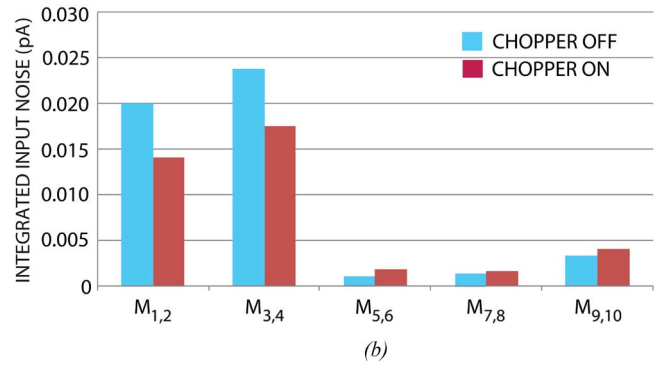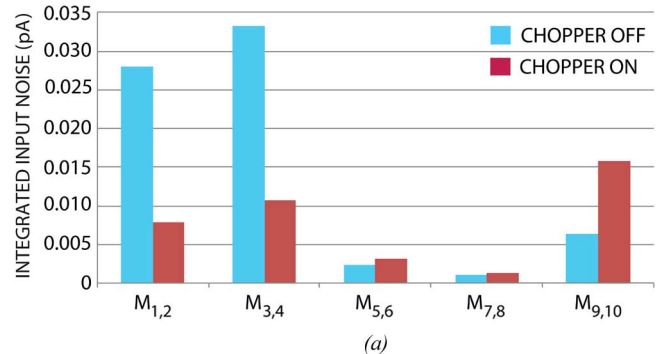| Transistor	W/L (μm)
$M_{1,2}$	$8 \times 1/0.4$
$M_{3,4}$	$1 \times 0.5/5$
$M_{5,6}$	$4 \times 0.5/4$
$M_{7,8}$	$8 \times 0.5/4$
$M_{9,10}$	$2 \times 0.5/0.5$
M_{11}	$4 \times 1/4$
M_S	$4 \times 1/0.13$

Fig. 7. Transimpedance amplifier noise summary: (a) flicker noise contributions, and (b) thermal noise contributions.

The OTA has a folded cascode topology as shown in Fig. 5. To reduce the effect of flicker noise, the amplifier utilizes input PMOS devices with a high aspect ratio and internal chopping. One set of the chopper switches is placed at the input of the OTA. Another set is placed at the folding nodes as depicted in Fig. 5. This significantly reduces the flicker noise and DC offsets caused by the input pair transistors, M_1 and M_2, and the NMOS current mirror transistors, M_3 and M_4. The size of the feedback capacitor is 10 pF. The chopper clock frequency can be set up to 20 kHz.

The simulated input-referred noise of the integrator for the cases where the chopper is disabled and enabled is shown in Fig. 6. The integrated input-referred noise from 0.01 Hz to 1 kHz is 0.12 pA when the chopper is disabled and 0.07 pA when the chopper is enabled. The integrator transistor sizes are shown in Table I. Contribution of each transistor to the total input-referred noise is shown in Fig. 7. When the chopper is disabled the main contributions are from the OTA current mirror transistors M_3 and M_4 and the input pair transistors M_1 and M_2. When the chopper is enabled, the current mirror transistors M_9 and M_{10} are the main contributors to the input-referred noise.

A. Circuit Implementation

The circuit diagram of the presented TIA is shown in Fig. 4. The TIA consist of a chopper-stabilized OTA with a capacitive feedback. The TIA operates in two phases. In phase one switch S is open. In this phase the OTA feedback ensures that the negative terminal of the OTA is at the working electrode potential. The input current is integrated over the feedback capacitor. This is the integrating phase of the TIA. In the next phase, switch S is closed to discharge the feedback capacitor. This removes any residual charge on the feedback capacitor at the end of one full cycle.
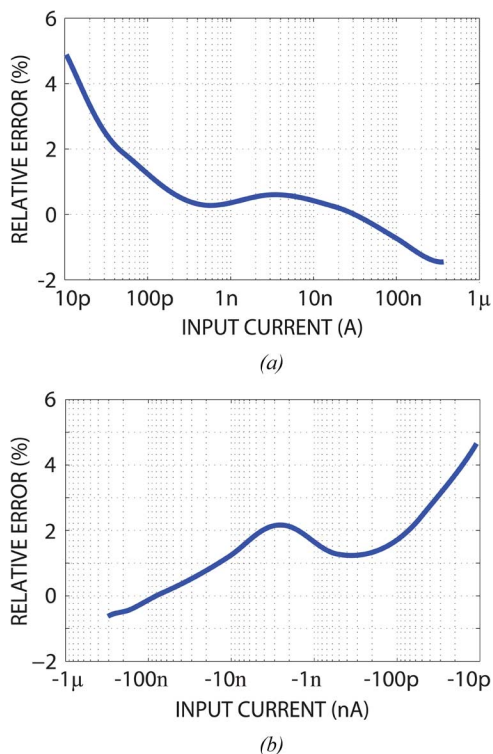
Fig. 8. Experimentally measured relative error of the output of the TIA for the input current of (a) 10 pA to 350 nA, and (b) -350 nA to -10 pA. The results are measured from one typical channel on one chip.

TABLE III
EXPERIMENTALLY MEASURED TRANSIMPEDANCE AMPLIFIER (TIA) AND CURRENT CONVEYER (CC) CHARACTERISTICS

	TIA	CC
Technology	$0.13\mu m$ CMOS	$0.13\mu m$ CMOS
Supply Voltage	1.2V	1.2V
Area	$80\mu m \times 60\mu m$	$100\mu m \times 100\mu m$
Sensitivity	135fA	8.6pA
Max Relative Error (10pA to 350nA)	5.1	8.0
Max Relative Error (10pA to 350nA)	4.8	7.8
Input Referred Noise (0.01Hz to 1kHz)	0.07pA	0.13pA
Charge Injection at 6kHz (Simulated)	221fA	53fA
Power Consumption		
Core Circuit	$1\mu W$	$2\mu W$
Biasing	$1\mu W$	$1\mu W$
Digital	$1\mu W$	$1\mu W$
Total	$3\mu W$	$4\mu W$
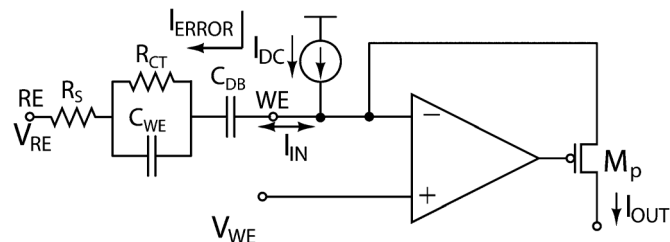
Fig. 10. Conventional pseudo-bidirectional current conveyer with a DC offset current.

B. Experimental Results

The transimpedance amplifier was fabricated in a 0.13 μm CMOS process with a 1.2 V supply and occupies an area of 80 μm $\times$ 60 μm.

The experimentally measured relative errors of the digital output for the input current swept between ± 10 pA and ± 350 nA are shown in Fig. 8. The relative error stays below 5 percent over the whole operating range. The TIA achieves a dynamic range of 10 pA to 350 nA. The lower limit is defined by the LSB of the on-chip ADC. The higher limit is defined by the input current that saturates the TIA.

Figs. 9(a), (b) show the experimentally recorded output current distribution for the input currents of 100 pA and 100 nA, respectively, measured from 16 channels on 16 chips (one channel per chip). The mean output current and the corresponding standard deviation are 80.89 pA and 6.9 pA, respectively, for the input current of 100 pA. They are 100.10 nA and 17.8 pA for input current of 100 nA. Table III summarizes the experimentally measured characteristics of the TIA.

III. CURRENT CONVEYER (CC)

Another common method to acquire a bidirectional current is to use a unidirectional current conveyer and to add a DC offset current to its input as shown in Fig. 10 [7]–[12]. This requires high resolution in the subsequent ADC and adds noise to the redox current. Also, depending on the WE impedance, a portion of the DC offset current, I_{ERROR}, can leak into the electrochemical cell and disturb the charge balance on the WE-electrolyte interface.
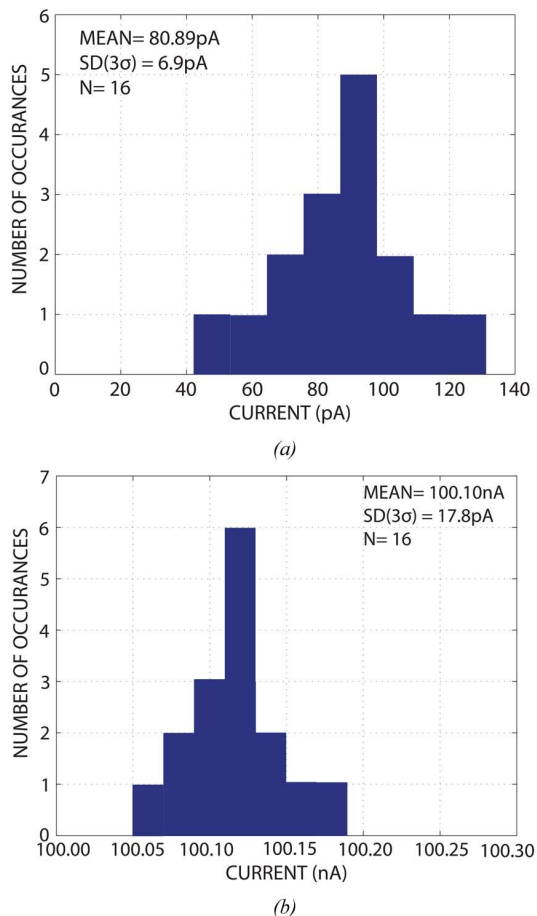

Fig. 9. Experimentally measured TIA output current of 16 channels (from 16 chips, one channel each) for the input current of (a) 100 pA, and (b) 100 nA.
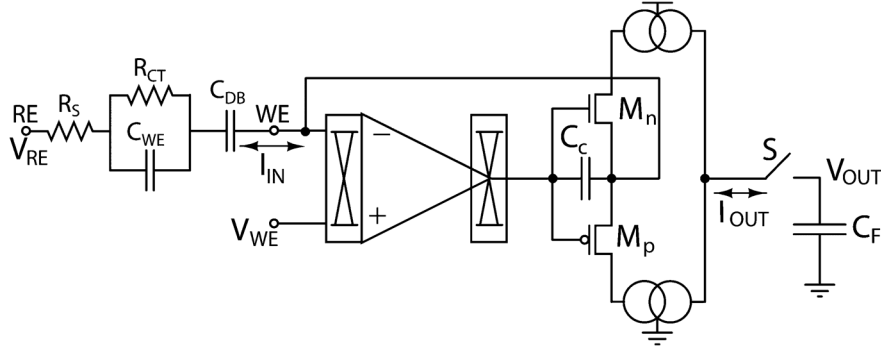
Fig. 11. Chopper-stabilized bidirectional current conveyer VLSI architecture.
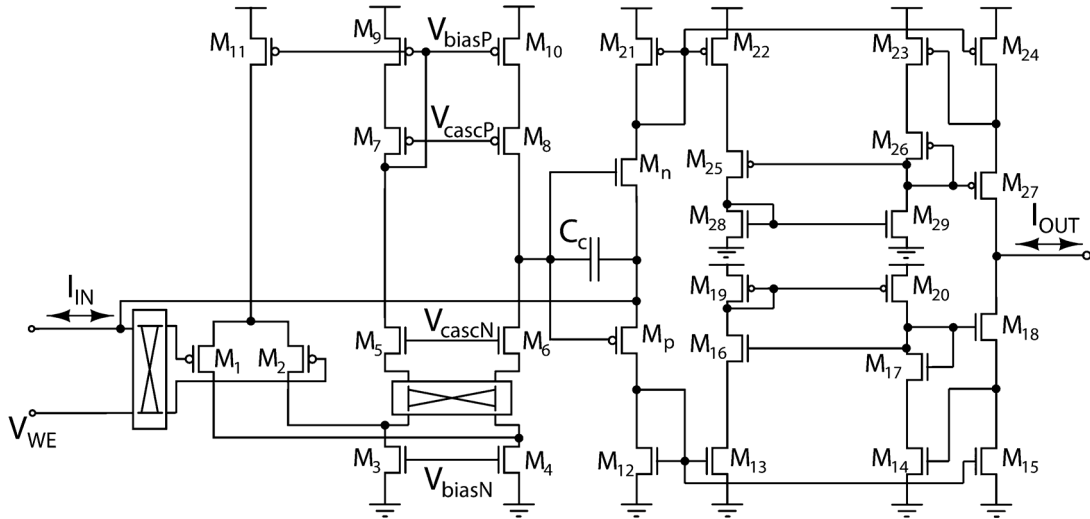

Fig. 12. Chopper-stabilized bidirectional current conveyer circuit schematic diagram.

A. Circuit Implementation

The top-level VLSI architecture of the presented bidirectional current conveyer is shown in Fig. 11. It is comprised of a PMOS and an NMOS transistors M_n and M_p connected in the feedback of the OTA. The negative feedback ensures a known potential at the working electrode is set by the voltage at the non-inverting input of the OTA. It also enables the current conveyer to source and sink input current without the need for a DC offset current. The currents through M_n and M_p are mirrored to the output of the current conveyer.Internal OTA chopping has been utilized to reduce the effect of its flicker noise. The current mirrors are implemented in a low-current regulated cascode topology to enable accurate current copying down to the pA level. To facilitate a comparative analysis with the TIA presented in Section IV, the output current is integrated on the load capacitor C_F of 10 pF and sampled.

The schematic diagram of the current conveyer is shown in Fig. 12. The OTA is implemented as a folded-cascode amplifier and the current mirrors are implemented as a low-current regulated cascode current mirror comprised of the transistors M_{12} to M_{20} and M_{21} to M_{29} [11]. The regulated cascode current mirrors ensure high precision and high output impedance of the current conveyer. The regulated current mirrors monitor I_{IN} through M_{13} and M_{22}. The input current is used to bias the regulating amplifiers consisting of transistors $M_{14}, M_{16}, M_{17}, M_{19}$,

M_{20} and $M_{23}, M_{25}, M_{26}, M_{28}, M_{29}$. The regulating amplifies sense the drain voltage of M_{15} and M_{24} through transistors M_{14} and M_{26} and adjust the gate voltage of M_{18} and M_{27} such that the drain-source voltage of M_{12}–M_{15} pair and M_{21}–M_{24} pair are equal pairwise thus ensuring accurate current copying down to pA level.

In more detail, for the NMOS section of the regulated cascode current mirror, transistors M_{14}, M_{17} and M_{20} form a common-source amplifier. The common-source amplifier forms a negative feedback loop with the help of source follower transistor M_{18}. This ensures a high impedance at the output of the current mirror. V_{ds} of M_{15} should be equal to V_{ds} of M_{12} to ensure accurate current copying. This is achieved as follows: the common-source amplifier is biased with the current I_{IN} using a (1:1) current mirror consisting of transistors M_{19} and M_{20}. The sizes of transistors M_{14} and M_{13} are equal to those of the transistors M_{12} and M_{15} respectively. Transistors M_{16} and M_{17} are sized such that they provide enough voltage drop to ensure that transistors $M_{12}, M_{13}, M_{14}, M_{15}$ have all the same V_{ds}. The value of the capacitor C_c is set to 0.5 pF to ensure OTA stability over the operating current range.

Similarly to the TIA, internal OTA chopping has been implemented to reduce the effect of both flicker noise and the input offset voltage. As shown in Fig. 12, chopper switches are placed at the input of the OTA. Another set is placed after the NMOS tail current source. This significantly reduces the flicker noise

TABLE II
CURRENT CONVEYER TRANSISTOR SIZING

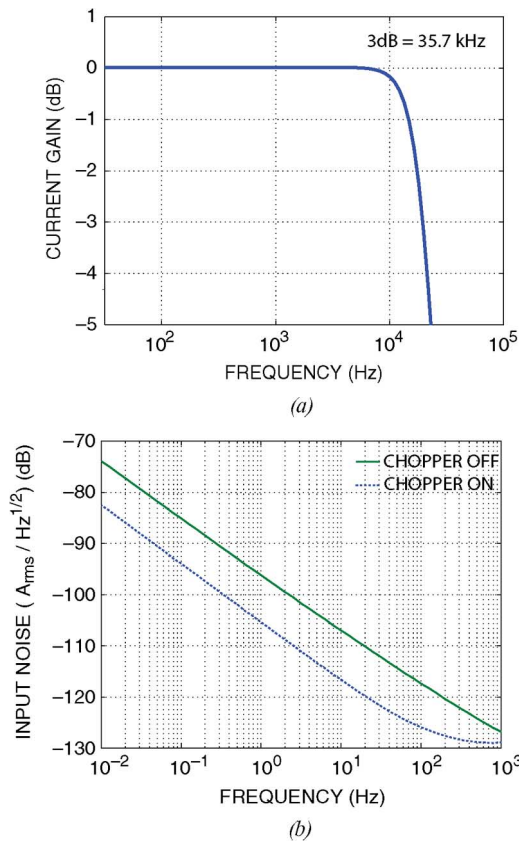| Transistor	W/L (μm)	Transistor	W/L (μm)
$M_{1,2}$	$8 \times 3/0.4$	$M_{16,17,18}$	$1 \times 0.5/4$
$M_{3,4}$	$1 \times 0.5/5$	$M_{19,20}$	$8 \times 0.3/5$
$M_{5,6}$	$4 \times 0.5/4$	$M_{21,22,23,24}$	$2 \times 0.4/8$
$M_{7,8}$	$8 \times 0.5/4$	$M_{25,26,27}$	$4 \times 0.7/3$
$M_{9,10}$	$2 \times 0.5/0.5$	$M_{28,29}$	$4 \times 0.3/4$
M_{11}	$4 \times 1/4$	M_p	$1 \times 1/1$
$M_{11,13,14,15}$	$1 \times 0.4/8$	M_n	$1 \times 0.4/4$

Fig. 13. (a) Simulated current conveyer AC response, and (b) simulated input-referred noise spectrum of the current conveyer from 0.01 Hz to 1 kHz.

and offsets due to the input pair transistors and the NMOS tail current source transistors. Minimum size switches are utilized to reduce the effect of charge injection into the working electrode. The current conveyer transistor sizes are shown in Table II.

In typical electrochemical sensing applications, the current conveyer operates in the frequency range of 0.01 Hz to 1 kHz. To achieve efficient flicker noise reduction, the chopper frequency needs to be higher than the input signal frequency. The chopper clock frequency was set to 10 kHz. As a result the current conveyer bandwidth should be higher compared to the case where no chopper stabilization is utilized. Simulated bandwidth of the current conveyer is shown in Fig. 13(a). The current conveyer achieves a 3 dB bandwidth of 35.7 kHz.

The simulated input-referred noise of the current conveyer for the cases where the chopper is disabled and enabled is shown in Fig. 13(b). The integrated-input referred noise from 0.01 Hz to 1 kHz is 0.27 pA for the case when the chopper is disabled and is 0.13 pA when the chopper is enabled.
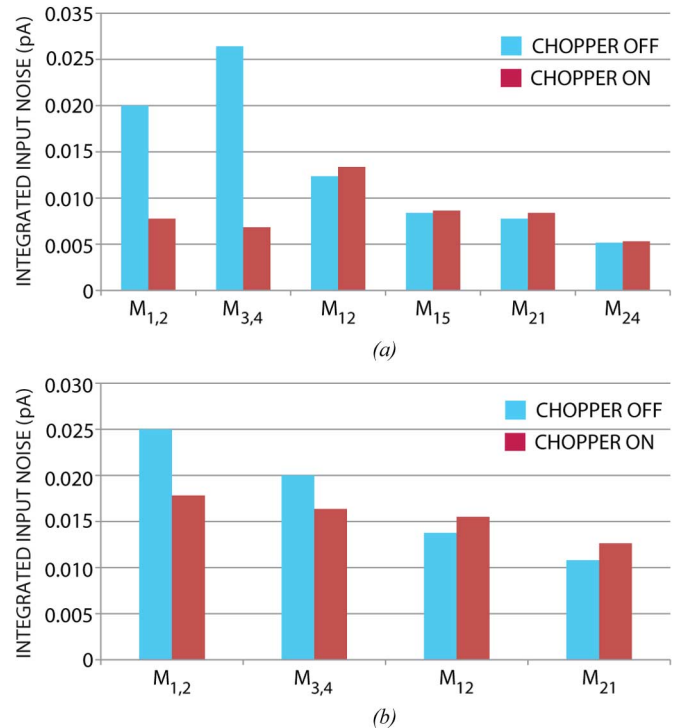

Fig. 14. Current conveyor noise summary: (a) flicker noise contributions, and (b) thermal noise contributions.

Contribution of each transistor to the total input-referred noise is shown in Fig. 14. When the chopper is disabled the main contributions are from the OTA current mirror transistors $M_{3,4}$ and the input pair transistors $M_{1,2}$. When the chopper is enabled, the current mirror transistors $M_{12,21,24,15}$ are the main contributors to the input-referred noise.

B. Experimental Results

The current conveyer was fabricated in a 0.13 μm CMOS process with a 1.2 V supply and occupies an area of 100 $\mu m \times$ 100 μm.

The experimentally measured relative errors of the digital output for the input current swept between ± 10 pA and ± 350 nA are shown in Fig. 15. The relative error stays below 8 percent over the whole operating range. The current conveyer achieves a dynamic range of 8.6 pA to 350 nA. The lower limit is defined by the ADC LSB and the higher limit is defined by the input current that saturates the current conveyer. Fig. 16 shows the experimentally recorded output current distribution for the input currents of 100 pA and 100 nA measured from 16 channels on 16 chips (one channel per chip). The mean output current and the corresponding standard deviation are 81.19 pA and 20.31 pA, respectively, for the input current of 100 pA. They are 100.21 nA and 29.0 pA for the input current of 100 nA. Table III summarizes the experimentally measured characteristics of the current conveyer.

IV. COMPARATIVE ANALYSIS

The electrical characteristics of TIA and CC are compared first. When the chopper is enabled, the TIA achieves and input-referred noise of 0.07 pArms and CC achieves an 0.13 pArms.
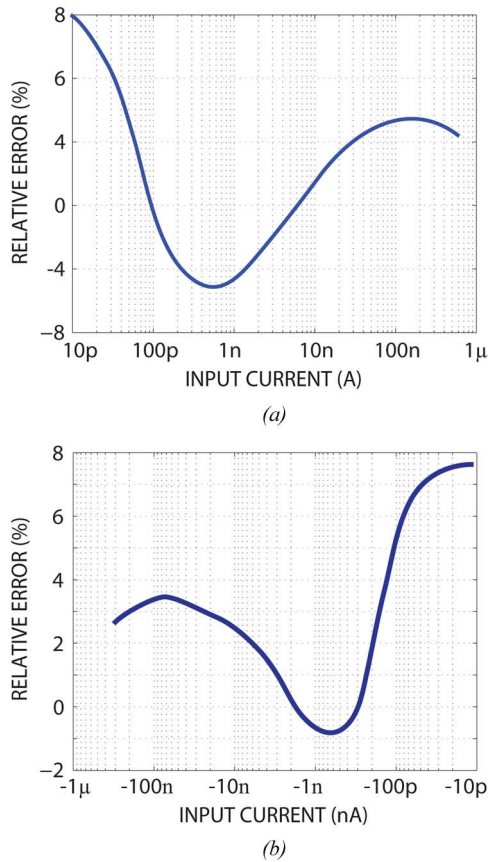
Fig. 15. Experimentally measured relative error of the output of the current conveyer for the input current of (a) 10 pA to 350 nA, and (b) -350 nA to -10 pA. The results are measured from one typical channel on one chip.

Fig. 16. Experimentally measured current conveyer output current of 16 channels (from 16 chips, one channel each) for the input current of (a) 100 pA and (b) 100 nA.

This is due to the fact that the TIA integrates noise over one sampling period.

The chip-to-chip output current variation of TIA, in Fig. 8, is lower compared to that of the CC design shown in Fig. 14. The variation in CC is mainly due to the mismatch in the output current mirrors. The maximum relative error of the output over the operating current range is 5 percent for the TIA and 8 percent for the CC. Mismatch in the regulated cascode current sources limits the linearity of the current conveyer. The mismatch in the regulated cascode current mirrors is due to the mismatch in the transistor pairs $M_{12}-M_{15}$ and $M_{21}-M_{24}$, as shown in Fig. 12. Dynamic element matching (DEM) can be employed to reduce the effect of the mismatch in the current mirrors.

To study the effect of charge injection into the working electrode, two sets of simulations were performed with the working electrode model in both Fig. 4 and Fig. 11 connected to the voltage V_{RE}. The average current integration into the working electrode, due to current integration and sampling, is calculated for the cases where the sampling frequency is varied from 1 kHz to 12 kHz and the chopping frequency is set to 20 kHz. As it can be seen from Figs. 17(a) and (b), the average current injected into the working electrode at 6 kHz for the case of the TIA is significantly higher compared to the average current injected by the CC.
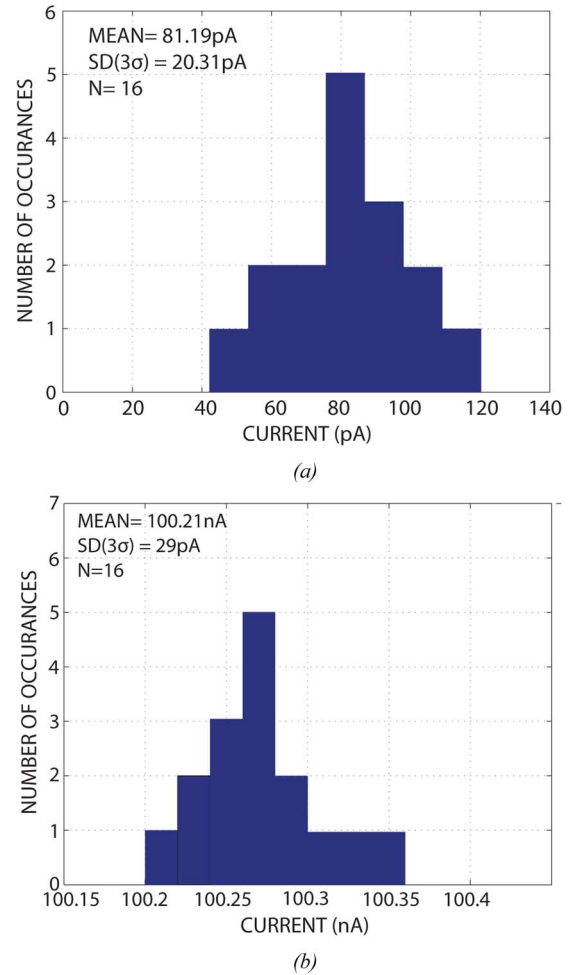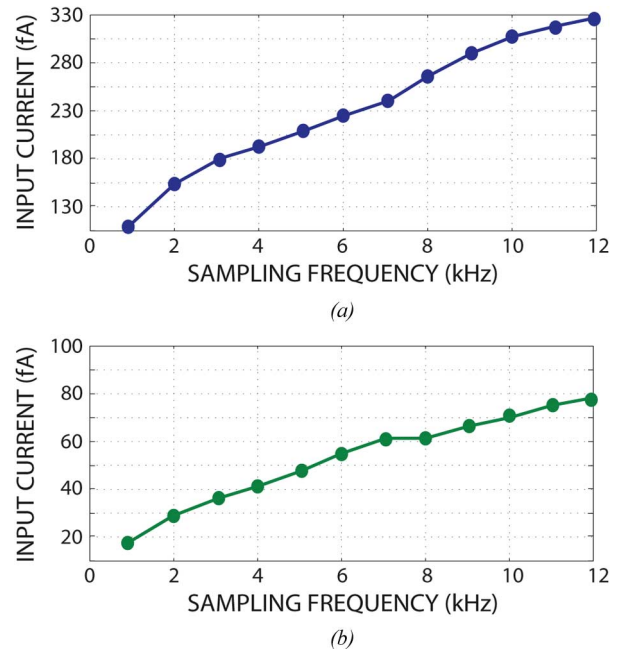

Fig. 17. Average current injected into the working electrode for (a) TIA and (b) CC.

Fig. 18. Cyclic voltammogram of 2 μM potassium ferricyanide in 1 M potassium phosphate buffer solution experimentally recorded with the transimpedance amplifier (TIA) and the current conveyer (CC) using a 50 μm $\times$ 50 μm gold electrode.
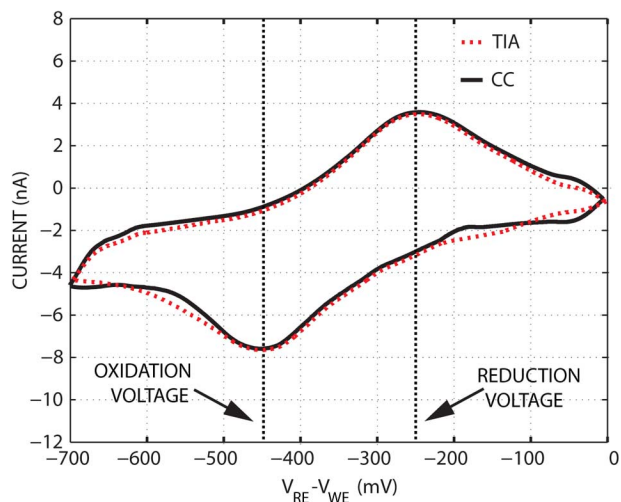

Fig. 19. Cyclic voltammogram of 2 μM potassium ferricyanide in 1 M potassium phosphate buffer solution experimentally recorded with the transimpedance amplifier (TIA) and the current conveyer (CC) using a 2 μm $\times$ 2 μm gold electrode.

To compare the performance of the TIA and CC in electrochemical sensing applications, two sets of CV scans of a DNA reporter, potassium ferricyanide, have been performed. Potassium ferricyanide $K_3[Fe(CN)_6]$ is commonly used in electrochemical sensing systems as a redox reporter [24]. Cyclic voltammetry recordings of 2 μM potassium ferricyanide in a 1 M potassium phosphate buffer (pH 7.3) have been carried out. A 100 mV/sec 0.7 V peak-to-peak CV waveform with 50 ms resting period was applied between a 55 μm $\times$ 55 μm on-chip gold working electrode and an off-chip Ag-AgCl reference electrode. The resulting CV curves recorded by the chopper-stabilized TIA and the chopper-stabilized CC are shown in Fig. 18. The CV curves for both TIA and CC show two distinct peaks at the reduction and oxidation voltages of potassium ferricyanide at -250 mV and -450 mV respectively. The measurements match as well.

Next the same set of CV recordings have been conducted using a 2 μm $\times$ 2 μm on-chip gold working electrode. The resulting CV curves recorded by the chopper-stabilized TIA and the chopper-stabilized CC are shown in Fig. 19. The CV curve for the CC shows two distinct peaks at the reduction and oxidation voltages of potassium ferricyanide, as expected. The CV curve for the TIA shows no reduction or oxidation peaks. In the TIA case the switching charge from switch S is injected into the working electrode. This disturbs the charge balance at the electrode-electrolyte interface thus affecting the electrochemical reaction required for reduction and oxidation of the potassium ferricyanide. As expected, this effect is more pronounced for smaller electrode size.

Both circuits inject small amount of charge generated by the chopper switches into the biosensor. This injected noise is negligibly small compared to the switching noise due to the feedback switch in the TIA and is due to the chopper switches mismatch.

V. CONCLUSIONS

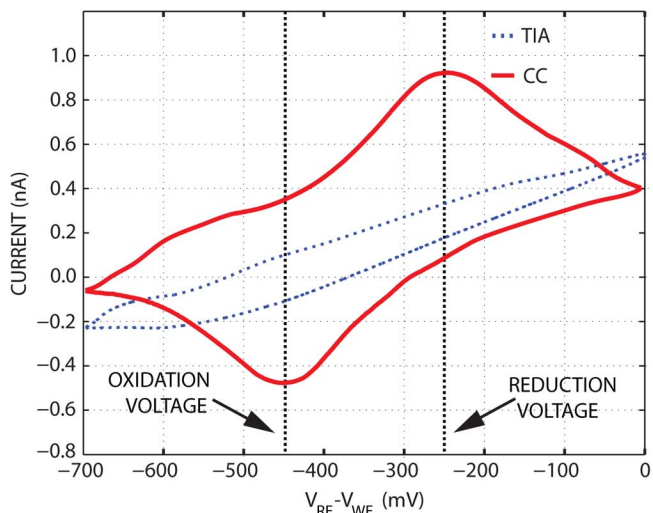Designs of two low-noise chopper-stabilized bidirectional current acquisition circuits for electrochemical sensing applications have been presented. The first design has a switched-capacitor transimpedance amplifier topology. The second one has a current conveyer topology. Both designs are implemented in a 0.13 μm CMOS technology. Electrical and electrochemical performance of both design has been characterized. The TIA and CC consume 3 μW and 4 μW from a 1.2 V supply, respectively. It is shown that the TIA marginally outperforms the CC for high-amplitude input currents. For small input currents corresponding to low concentration of biochemicals the CC is the preferred choice as it better isolates the working electrode from current injection.

REFERENCES

[1] M. Roham, M. P. Garris, and P. Mohseni, "A wireless IC for time-share chemical and electrical neural recording," *IEEE J. Solid-State Circuits*, pp. 3645–3658, 2009.

[2] R. Genov, M. Stanacevic, M. Naware, G. Cauwenberghs, and N. Thakor, "16-channel integrated potentiostat for distributed neurochemical sensing," *IEEE Trans. Circuits Syst. I*, vol. 53, no. 11, pp. 2371–2376, Nov. 2006.

[3] T. G. Drummond, M. G. Hill, and J. K. Barton, "Electrochemical DNA sensors," *Nature Biotechnol.*, vol. 21, no. 10, pp. 1192–1199, Oct. 2003.

[4] M. Schienle, C. Paulus, A. Frey, F. Hofmann, B. Holzapfl, P. S. Bauer, and R. Thewes, "A fully electronic DNA sensor with 128 positions and in-pixel A/D conversion," *IEEE J. Solid-State Circuits*, vol. 39, no. 12, pp. 2438–2445, 2004.

[5] C. Yang, Y. Huang, B. L. Hassler, R. M. Worden, and A. J. Mason, "Amperometric electrochemical microsystem for a miniaturized protein biosensor array," *IEEE Trans. Biomed. Circuits Syst.*, vol. 3, no. 3, pp. 160–168, 2009.

[6] F. Heer, M. Keller, G. Yu, J. Janata, M. Josowicz, and A. Hierlemann, "CMOS electro-chemical DNA-detection array with on-chip ADC," in *Proc. IEEE Int. Solid-State Circuits Conf. (ISSCC)*, 2008, pp. 168–169.

[7] A. Hassibi and T. H. Lee, "A programmable 0.18 μm CMOS electrochemical sensor microarray for bimolecular detection," *IEEE Sensors J.*, vol. 6, pp. 1380–1388, 2006.

[8] B. Jang, P. Cao, A. Chevalier, A. Ellington, and A. Hassibi, "A CMOS fluorescence-based biosensor microarray," in *Proc. IEEE Int. Solid-State Circuits Conf. (ISSCC)*, Feb. 2009, pp. 436–437.

[9] A. Hassibi, H. Vikalo, J. L. Riechmann, and B. Hassibi, "Real-time DNA microarray analysis," *Nucl. Acids Res.*, vol. 37, no. 20, pp. 1–12, Aug. 2009.

[10] P. M. Levine, P. Gong, R. Levicky, and K. L. Shepard, "Active CMOS sensor array for electrochemical biomolecular detection," *IEEE J. Solid-State Circuits*, vol. 43, no. 8, pp. 1859–1871, 2008.

[11] A. Yang, S. R. Jadhav, R. M. Worden, and A. J. Mason, "Compact low-power impedance-to-digital converter for sensor array microsystems," *IEEE J. Solid-State Circuits*, vol. 44, no. 10, pp. 2844–2855, 2009.

[12] A. Manickam, A. Chevalier, M. McDermortt, A. D. Ellington, and A. Hassibi, "A CMOS electrochemical impedance spectroscopy biosensor array for label-free biomolecular detection," in *Proc. IEEE Int. Solid-State Circuits Conf. (ISSCC)*, 2010, pp. 130–131.

[13] P. Kim, N. Kohli, A. Mason, R. M. Worden, and R. Ofoli, "An electrochemical interface for integrated biosensors," in *IEEE Int. Conf. Sensors*, Oct. 2003.

[14] A. Mason, Y. Huang, C. Yang, and J. Zhang, "Amperometric readout and electrode array chip for bioelectrochemical sensors," in *Proc. IEEE Int. Symp. Circuits and Systems (ISCAS)*, May 2007, pp. 3562–3565.

[15] H. Jafari and R. Genov, "Bidirectional current conveyer with chopper stabilization and dynamic element matching," in *Proc. IEEE Int. Symp. Circuits and Systems (ISCAS'2012)*, 2012.

[16] H. S. Narula and J. G. Harris, "A time-based VLSI potentiostat for ion current measurement," *IEEE Sensors J.*, vol. 6, pp. 239–247, 2006.

[17] M. Ahmadi and G. Jullien, "Current-mirror-based potentiostats for three-electrode amperometric electrochemical sensors," *IEEE Trans. Circuits Syst. I*, vol. 56, pp. 1339–1348, 2009.

[18] S. Hwang and S. Sonkusale, "CMOS VLSI potentiostat for portable environmental sensing applications," *IEEE Sensors J.*, vol. 10, pp. 820–821, 2010.

[19] S. Ayers, K. D. Gillis, M. Lindau, and B. A. Minch, "Design of a CMOS potentiostat circuit for electrochemical detector arrays," *IEEE Trans. Circuits Syst. I*, vol. 54, no. 4, pp. 736–744, April 2007.

[20] A. Zeki and H. Kuntman, "Accurate and high output impedance current mirror suitable for CMOS current output stages," *IEEE Sensors J.*, vol. 6, pp. 1380–1388, 2012.

[21] T. Kurashina, S. Ogawa, and K. Watanabe, "A high performance class AB current conveyer," in *IEEE Int. Conf. Electronics, Circuits and Systems*, 1998, vol. 3, pp. 143–146.

[22] D. Kim, B. Goldstein, W. Tang, F. Sigworth, and E. Culurciello, "Noise analysis and performance comparison of low current measurement systems for biomedical applications," *IEEE Trans. Biomed. Circuits Syst.*, vol. 99, no. 1, 2012.

[23] J. Xu, F. Q. Fan, J. H. Huijsing, C. V. Hoof, R. F. Yazicioglu, and K. A. A. Makinwa, "Measurement and analysis of input current noise in chopper amplifiers," in *Proc. Eur. Solid-State Circuits Conf. (ESSCIRC)*, 2012, pp. 81–84.

[24] H. M. Jafari, L. Soleymani, K. Abdelhalim, E. H. Sargent, S. O. Kelley, and R. Genov, "Nanostructured CMOS wireless ultra-wideband label-free DNA analysis SoC," in *IEEE Symp. VLSI Circuits, Dig. Tech. Papers*, 2012, pp. 69–70.

Hamed Mazhab Jafari (SM'11) received the B.Eng. and M.A.Sc. degrees in electrical engineering from McMaster University, Hamilton, ON, Canada, in 2004 and 2006, respectively, and is currently pursuing the Ph.D. degree in electrical and computer engineering at the University of Toronto, Toronto, ON, Canada. His M.A.Sc. thesis focused on low-power ultra-wideband CMOS front end and ultra-widebands antennas. He is currently working toward the Ph.D. degree at uiversity of Toronto, Toronto, Canada. His Ph.D. dissertation fcous is on CMOS DNA analysis SoC.

He has held internship positions at Kapik Integration, where he worked on low-power mixed signal circuits. Since 2011, he has been with Snowbush IP, Toronto, ON, Canada, where he focuses on research and development of next-generation high-speed wireline communication systems.

Roman Genov (S'96–M'02) received the B.S. degree (first rank) in electrical engineering from Rochester Institute of Technology, Rochester, NY, USA, in 1996, and the M.S. and Ph.D. degrees in electrical and computer engineering from Johns Hopkins University, Baltimore, MD, USA, in 1998 and 2002, respectively.

Dr. Genov held engineering positions at Atmel Corporation, Columbia, MD, in 1995 and Xerox Corporation, Rochester, NY, in 1996. He was a visiting researcher in the Laboratory of Intelligent Systems at Swiss Federal Institute of Technology (EPFL), Lausanne, Switzerland, in 1998 and in the Center for Biological and Computational Learning at Massachusetts Institute of Technology, Cambridge, MA, in 1999. He is presently an Associate Professor in the Department of Electrical and Computer Engineering at the University of Toronto, Canada. His research interests include analog and digital VLSI circuits, systems and algorithms for energy-efficient signal processing with applications to electrical, chemical and photonic sensory information acquisition, biosensor arrays, brain-silicon interfaces, parallel signal processing, adaptive computing for pattern recognition, and implantable and wearable biomedical electronics.

Dr. Genov received Canadian Institutes of Health Research (CIHR) Next Generation Award in 2005, Brian L. Barge Award for excellence in microsystems integration in 2008, DALSA Corporation Award for excellence in microsystems innovation in 2006 and 2009, and Best Paper Award on sensors and Best Student Paper Award, both at the IEEE International Symposium on Circuits and Systems in 2009. He is an Associate Editor of IEEE Transactions on Biomedical Circuits and Systems, IEEE Transactions on Circuits and Systems II: Express Briefs, and IEEE Signal Processing Letters.